Soft Matter

ARTICLE TYPE

Cite this: DOI: 00.0000/xxxxxxxxxx

Supporting information: Dilute polyelectrolyte solutions: recent progress and open questions†

Carlos G. Lopez[a], Atsushi Matsumoto[b], and Amy Q. Shen[c]

Contents

[a] *Institute of Physical Chemistry, RWTH Aachen University, Aachen, 52056, Germany, European Union*
[b] *Department of Applied Chemistry and Biotechnology, Graduate School of Engineering, University of Fukui, 3-9-1 Bunkyo, Fukui City, Fukui 910-8507, Japan*
[c] *Micro/Bio/Nanofluidics Unit, Okinawa Institute of Science and Technology Graduate University, 1919-1 Tancha, Onna-son, Okinawa 904-0495, Japan*
E-mail:(CGL) lopez@pc.rwth-aachen.de; (AM) atsushi5@u-fukui.ac.jp; (AQS) amy.shen@oist.jp

1 Phase behaviour

1.1 Variation of the theta temperature with added salt concentration

In Fig. 1, the reciprocal of T_c, where T_c corresponds to the temperature at the maximum of the T versus c curve in the phase diagram, is depicted as a function of the inverse square root of the degree of polymerization ($N^{-1/2}$). Similar to neutral polymers, linear relationships are apparent.[1] The intercept signifies the reciprocal of theta temperature (θ^{-1}), while the slope is linked to the enthalpic component of the χ parameter.

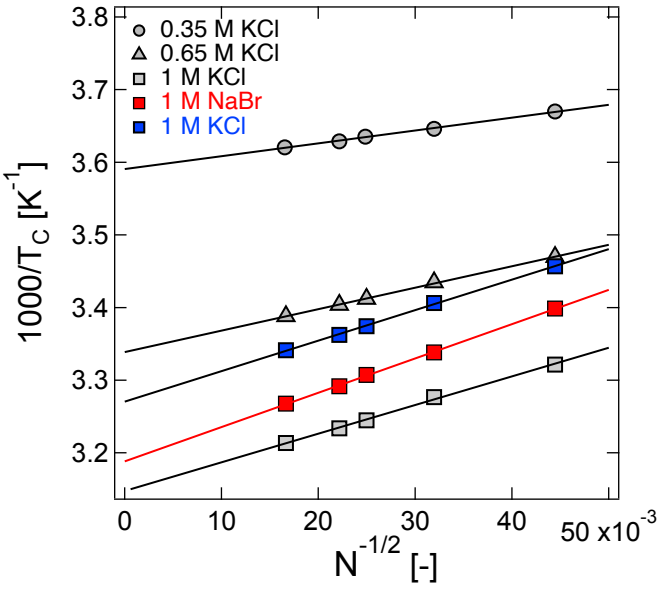

Fig. 1 Inverse critical phase separation temperature, obtained from maxima in T_p vs. c diagrams, plotted as a function of the inverse of the square root degree of the degree of polymerisation. Lines are best fits to linear functions. Data are extracted from [2].

The theta temperature of polystyrene sulfonate has been reported by several authors.[3–6] The degree of sulfonation of the PSS samples was only reported by Hirose (100%) and Nordmeier (84%). Other studies used PSS polymers synthesised through the sulfonation of polystyrene, implying a degree of sulfonation below 100%. The θ temperature from Raziel's data was estimated by interpolating the point at which $A_2 = 0$ for the samples listed in Tab. 4 of ref. [6]. Fig. 2 shows the θ temperature dependence on the added salt concentration c_s across diverse findings documented in the literature. For comparison, results for polyacrylic acid at various degrees of neutralisation[7,8] and other polyelectrolytes are also depicted in Fig. 2. While a linear dependence is discernible across all instances, it's worth noting that these observations are confined to a relatively narrow span of added salt concentrations.

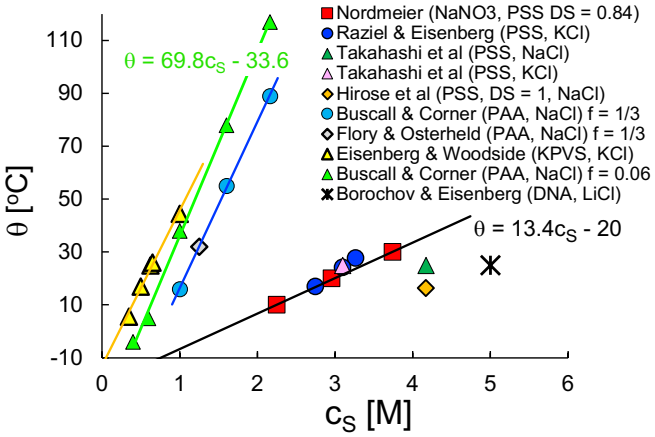

Fig. 2 The theta temperature is plotted against the added salt concentration for polystyrene sulfonate, polyacrylic acid with various degrees of neutralisation, DNA, and polyvinyl sulfate (PVS). The polymer and the type of added salt is shown in the legend. Data are obtained from refs. [2–9]. The equations for the black and green lines are given in the figure.

1.2 Phase maps

The phase map of fully neutralised sodium polyacrylate in aqueous solutions with added calcium chloride is plotted in Fig. 3(a). In the high polymer concentration region, the critical salt concentration c_s required for phase separation is $\simeq 0.33c$, which is qualitatively similar to the behaviour observed for trivalent ions in Fig. 6b of the main text. At low polymer concentrations, the critical c_s decreases with increasing polymer concentration. The increase in c_s at low polymer concentration has been observed in other studies[13]. However, other systems, including carboxymethyl cellulose in the presence of $CaCl_2$, $BaCl_2$ or $ZnCl_2$ or polystyrene sulfonate with added $BaCl_2$ display a constant value of c_s at lower polymer concentrations.[14–17]

Fig. 3(b) shows the phase boundaries of fully neutralised sodium polyacrylate in an aqueous solution containing 0.01 M NaCl, with different added alkaline earth chlorides. Data are extracted from ref. [11]. For the 90% neutralised polymethacylic acid data that were discussed in section 3.1 of the main manuscript, the type of cation was found to have a weaker effect on the position of the phase boundary. Fig. 3(c) considers the influence of NaCl concentration on the phase boundary for added $CaCl_2$. As the NaCl concentration increases, a larger concentration of $CaCl_2$ is required for precipitation, and the slope of the phase boundary in the low c region decreases.

Fig. 4(a) illustrates the temperature-polymer concentration phase diagram of polystyrene sulfonate in the pres-

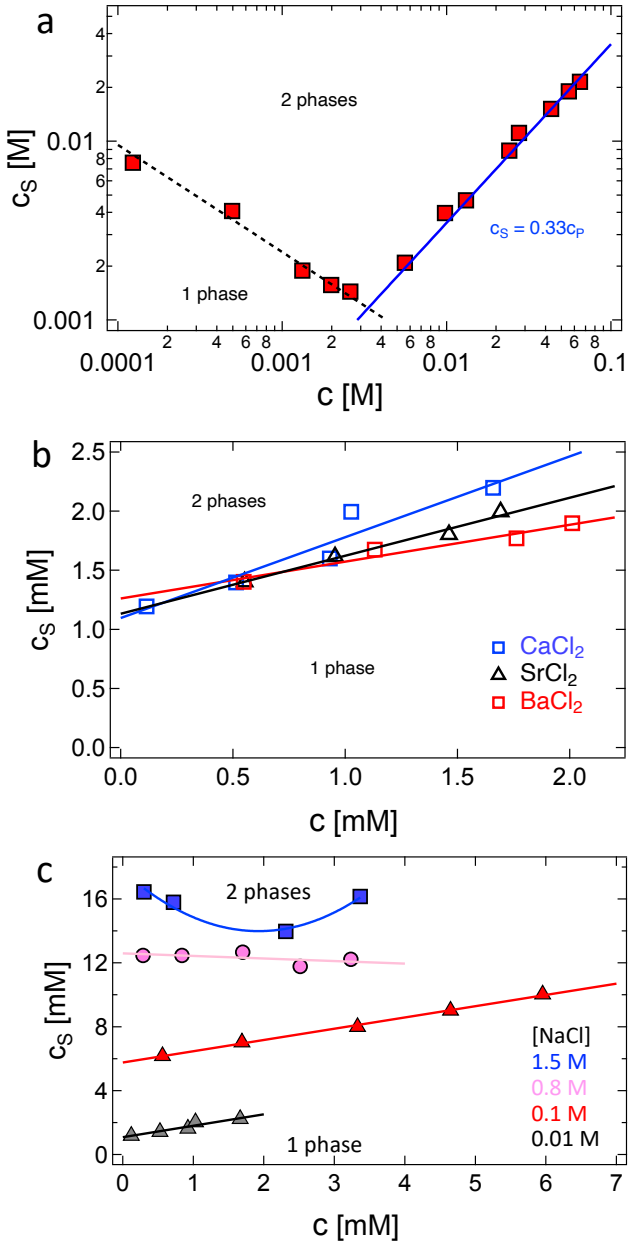

Fig. 3 a: $CaCl_2$ concentration required for phase separation of fully neutralised polyacrylic acid in DI water as a function of NaPA concentration c. Data are obtained from ref. [10]. The solid line is $c_s = c/3$, the dashed line is the best-fit power-law of $c_s = 3.8 \times 10^{-5} c^{-0.6}$. b: alkaline earth concentration required for phase separation of NaPA in 0.01 M NaCl aqueous solutions. Data are from ref. [11] c: $CaCl_2$ concentration required for phase separation of NaPA in different aqueous NaCl solutions, with different concentrations shown on the legend. Lines are guides to the eye. Data are from ref. [12].

ence of barium chloride,[16] displaying similar shape (qualitatively) to that of PVS in the presence of monovalent salts as discussed in section 3.1 of the main text, but the concentrations of added salt required for precipitation are much

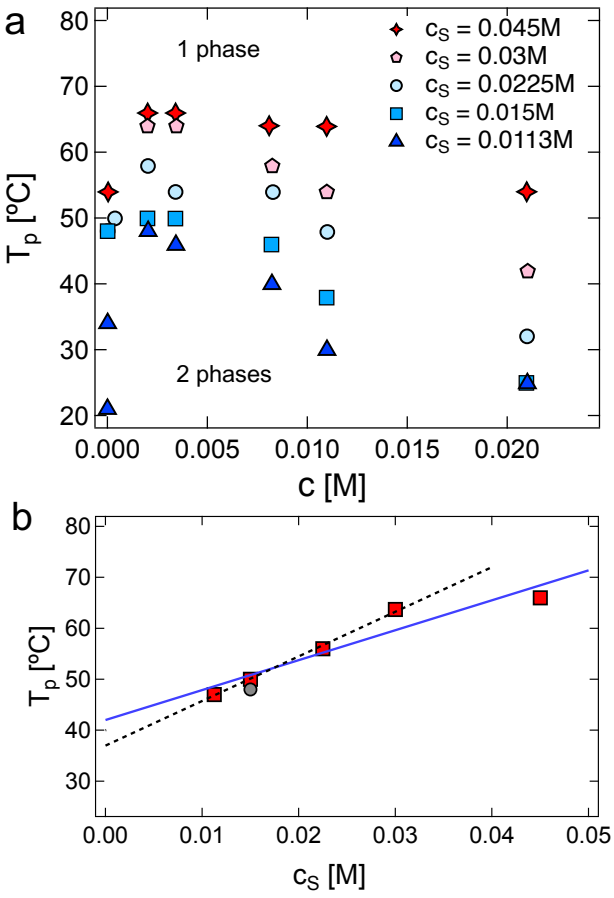

Fig. 4 a: Phase separation temperature of sodium polystyrene sulfonate with $N \simeq 580$ in aqueous solutions with different concentrations of added $BaCl_2$ (indicated on the legend), as a function of the polymer concentration. Data are extracted from ref. [16] b: Phase separation temperature at $c = 0.0027$ M, corresponding to the maxima in part a (squares), as a function of added $BaCl_2$ concentration (red squares). Circle represents the maximum in $T - c$ diagram for NaPSS with $N \simeq 500$, DS = 0.94 from ref [18]. Blue line is the best fit for all data points, and dashed back line is the best fit excluding the highest c_s datum.

lower. The phase separation temperature at $c = 2.7$ mM is plotted as a function of added $BaCl_2$ concentration in Fig. 4(b). As this concentration corresponds approximately to the maxima for the various curves, these values serve as a coarse estimate for the θ temperature of the system.* For comparison, we also add a datum extracted from ref. [18] for NaPSS with $M_w \simeq 110$ kg/mol. The phase diagram for this sample has a maximum at $c \simeq 0.005$ M. The result by Kanai and Muthukumar agrees well with the data of Prabhu. Note that a linear fit to the data gives $\theta \simeq 30 - 40$ °C in DI water, which is clearly incorrect, as the theta tem-

* Lacking molar mass dependent data to extrapolate to the $N \to \infty$ limit, we neglect the correction for the finite molar mass of the system.

perature is far below room temperature for salt-free conditions. The T_p vs. c_s curve is therefore expected to deviate from the linear trend and sharply bend downwards at low added salt concentrations.

2 Shear rate dependency of viscosity in dilute solutions

Yanaki and Yamaguchi[19] measured the intrinsic viscosity of sodium hyaluronate as a function of shear rate for different molar masses. In agreement with Fixman's theory,[20] they found that for a fixed value of the reduced shear rate K_η, more pronounced reduction in $[\eta](\dot{\gamma})/[\eta]$ occurred with increasing molar masses. Within this context, Fixman's theory enables the extraction of the viscosity expansion factor α_η from the shear rate-dependent behavior of $[\eta]$. In Fig. 5, we compare the values of α_η estimated from Eq. 39 of the main text with the more reliable estimates obtained in section 3.11. This analysis reveals that Fixman's theory tends to overestimate the excluded volume parameter.

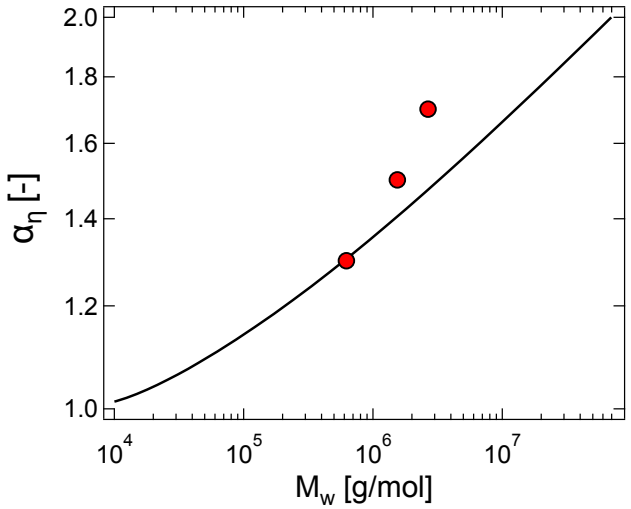

Fig. 5 Expansion factor for the intrinsic viscosity $\alpha_\eta = ([\eta]/[\eta]_0)^{1/3}$, where $[\eta]_0$ is the intrinsic viscosity of the chain without involving excluded volume as a function of molar mass for NaHy in 0.2 M NaCl solution. Black line is calculated from the expanded worm-like chain model, using the parameters reported in ref [21]. Red squares are values estimated by Yanaki and Yamaguchi[19] through fitting Fixman's model to the shear rate-dependent behavior of intrinsic viscosity.

3 The temperature and molar mass effects on the maximum reduced viscosity

The reduced viscosity η_{red} is a dimensionless quantity that is calculated by dividing the viscosity of a solution by the viscosity of the solvent. Reduced viscosity provides a way to remove the inherent differences in viscosity between solvents, while focusing on the impact of solute molecules or polymers on the flow properties of the solution.As discussed in the main text, for polyelectrolyte solutions, it is well-known that the dependence of η_{red} on the polymer concentration exhibits a maximum at c_{max} in the dilute or semidilute regimes. Here we examine the temperature and molar mass dependence of c_{max}.

3.1 Dependence of c_{max} on temperature

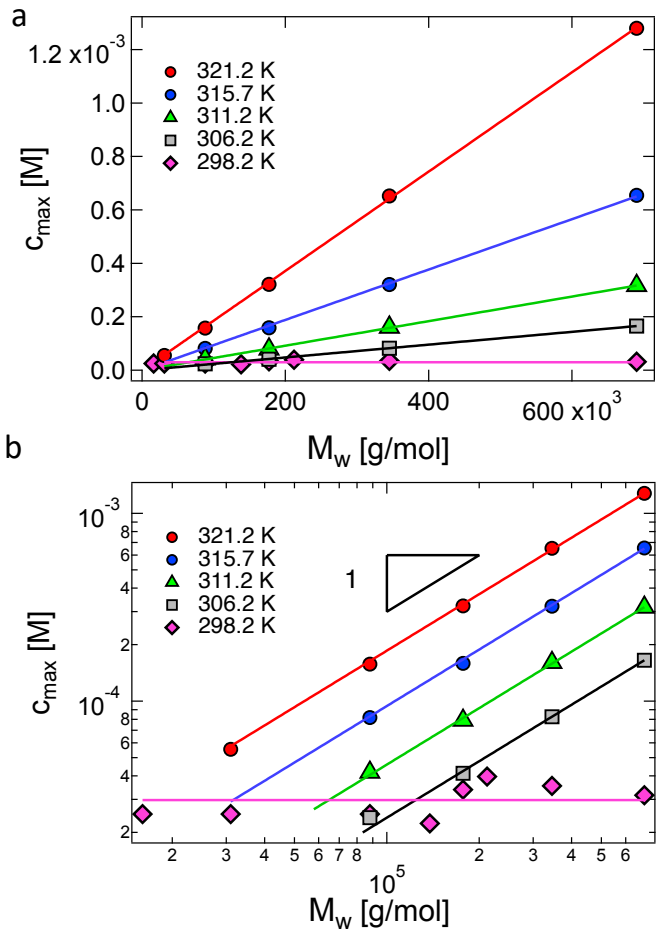

Fig. 6 Concentration at which reduced viscosity has a local maximum as a function of molar mass for Cohen et al's samples. Data are from [22] for $T = 298$ K and [23] for other temperatures. Panels a and b plot the same data but in linear and logarithmic axis respectively. The lines are power-laws of 0 for $T = 298$ K and 1 for all other temperatures. For 298 K the best-fit exponent is $\simeq 0.1$, for all other temperatures, the best fit exponent is 1 within error.

Cohen et al found that the reduced viscosity of dilute NaPSS solutions in low added salt aqueous solutions is strongly dependent on temperature.[23] A variation of 20 K could induce changes in the reduced viscosity of an order of magnitude at low polymer concentrations. Such behaviour was found to strongly contradict their interpretation of the viscosity peak using mode coupling theory[22] presented in

their earlier study. Fig. 6(a) plots the variation of the concentration at the maximum η_{red} (c_{max}) against the molar mass at different temperatures, combining the data from refs. [22] (for 298 K) and [23] (for other temperatures). The findings suggest that the location of the maximum η_{red} is $N-$independent only at around $T \simeq 298$ K, representing a molar mass-independent maximum. A similar plot, excluding the data at 298 K was presented in Fig. 4 of ref. [23], where it was noted that '*At 300 K, the dependence of $C_{p,max}$ [c_{max} in our notation] on the molecular weight is so small that it is within the accuracy of our measurements, which is consistent with our previous report*'. Re-plotting their data in double logarithmic axis (Fig. 6b) however revealed a different trend with temperature and molar mass. In this representation, no gradual transition in the slope is observed and instead a transition occurs from $c_{max} \propto N$ to $c_{max} \propto N^0$, where the critical N for the transition decreases with increasing temperature.

A separate report by Yang et al.[24] showed that the reduced viscosities of dilute solutions NaPSS ($N \simeq 350$) in low added salt aqueous solution display only a weak dependence on temperature for $T = 303 - 318$ K, in the $c \simeq 0.01 - 0.001$ M concentration range. Their data do not allow for a clear evaluation of the dependence of c_{max} on temperature. A study by Essafi et al.[25] for NaPSS with high degree of sulfonation also reveals a very weak dependence of η_{red} on temperature. Both reports therefore suggest that at high concentrations, the temperature dependence of the reduced viscosity becomes weak, which is not observed in figure 1 of Cohen et al.'s study.[23]

3.2 Dependence of c_{max} on molar mass

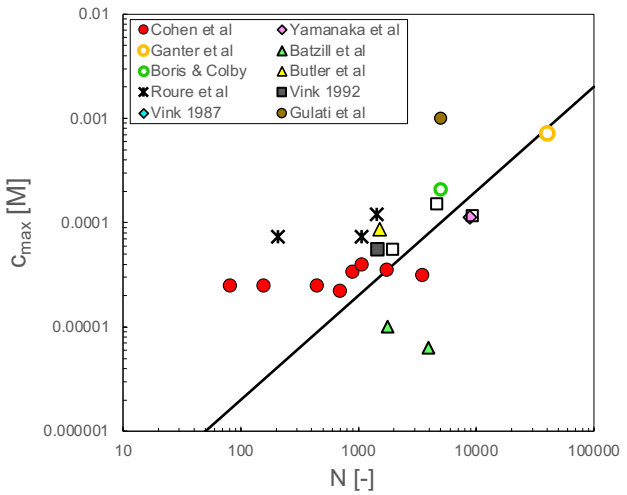

Fig. 7 Dependence of c_{max} on NaPSS degree of polymerisation for samples in DI water. The line corresponds to a power-law with an exponent of 1. Data are from refs. [22,26–34].

To further test the possible influence of the degree of polymerisation on c_{max}, we collect literature data measured at $T = 298$ K in Fig. 7. The scatter in the data is too strong to draw any solid conclusions. If the data of Batzill et al. are ignored, a general increase of c_{max} with N may be observed for $N \gtrsim 2000$, which is consistent with the trends observed for Cohen et al.'s data in Fig. 6(b). In any case, it is clear that further experimental work on the temperature dependence of the dilute solution viscosities of NaPSS is needed to resolve the issues raised here. We note that the mode coupling theory of Borsali et al.[35] predicts $c_{max} \propto N^{-1}$, which is not borne out by the data.

4 Scaling of intrinsic viscosity with charge density

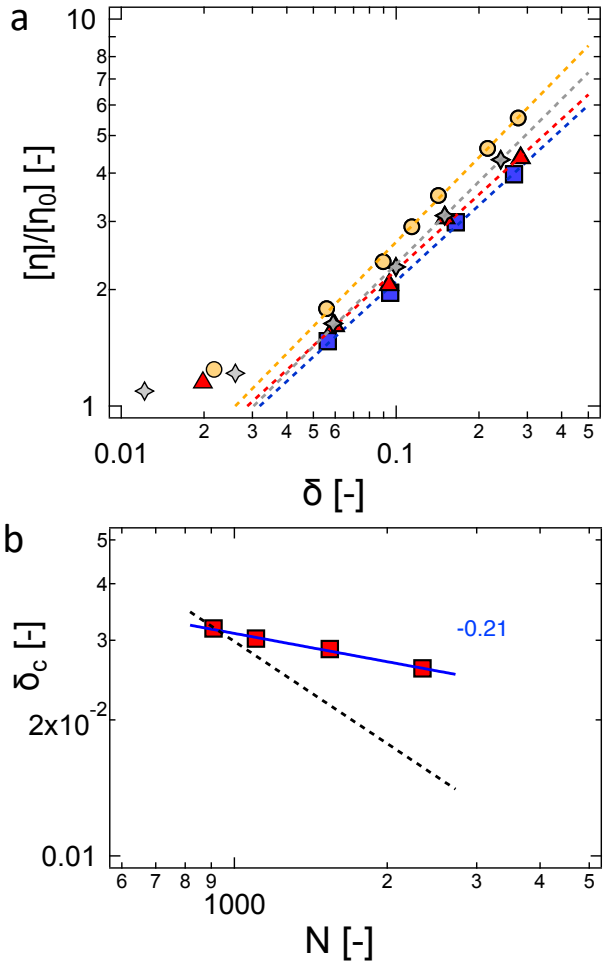

Fig. 8 a: The intrinsic viscosity of PVA co-polymer as a function of the fraction of charged groups, normalised by $[\eta]$ for the neutral polymer. Data are from ref. [36]. The lines are power-law fits to the high δ region. b: The critical charge fraction f_c, obtained from the intercept of power-law fits in Fig. 8a with $[\eta]/[\eta_0] = 1$, as a function of the degree of polymerisation N. The solid line is the best fit power-law and dashed line is the scaling prediction for the theta solvent case (exponent of $-3/4$).

The intrinsic viscosity of polyvinyl alcohol (PVA) copolymer with varying fraction of ionic groups, normalised to the value of the non-ionic polymer is plotted in Fig. 8(a) as a function of the charged group fraction (δ). Polymers with different degree of polymerisation are considered, all of which show the same scaling of $[\eta]/[\eta_0] \propto \delta^{0.8}$ in the high δ region. This exponent is $\simeq 30\%$ smaller than the value found in the main paper for polyacrylic acid with different degrees of neutralisation. The scaling theory expects a stronger exponent of 1.41, as discussed in the main manuscript.

The power-laws in the high δ region of figure 8a intercept with $[\eta]/[\eta_0] = 1$ at a critical charge fraction δ_c, which corresponds to the point at which electrostatics start to perturb the conformation of the polymer chains. The parameter δ_c is plotted as a function of degree of polymerisation in Fig. 8(b), where a weak power-law of $\delta_c \propto N^{-0.2}$ is observed. This contrasts with the much stronger exponent of $\delta_c \propto N^{-3/4}$ expected by the scaling model for polyelectrolytes in θ solvent for the backbone, as shown by the dashed black line where the pre-factor has chosen to match the value of δ_c for the lowest N sample.

5 Concentration dependence of shear viscosity in dilute polyelectrolyte solutions

The shear viscosity in dilute polymer solutions is often fitted to the Huggins equation:[37]

$$\frac{\eta_{sp}}{c} = [\eta] + k_H[\eta]^2 c, \quad (1)$$

where k_H is the Huggins coefficient, η_{sp} the specific viscosity, [η] the intrinsic viscosity and c the polymer concentration.

As discussed in the main text, equation 1 applies to polyelectrolytes in low ionic strength media only at extreme dilution. It is not clear, given the available data, whether the validity of the Huggins equation in solvents without added salt sets in only when the concentration of free counterions is smaller than those of added or residual salt (i.e. $fc \lesssim 2c_s$). Some studies, for example by Yamanaka et al.'s[38] suggest that the Huggins equation can hold for $fc \gtrsim 2c_s$ in some cases.

Another popular method to fit the viscosity of dilute neutral polymer solutions is the Kraemer's equation:[39]

$$\frac{ln(\eta_{rel})}{c} = [\eta] + k_K([\eta])^2 c, \quad (2)$$

where k_K is the Kraemer's constant.

In the $[\eta]c \ll 1$ limit, Eqs. 1 and 2 are equivalent, with

$$k_H = k_K + 1/2$$

Gosteva et al.[40] pointed out that the Kraemer plot ($\frac{ln(\eta_{rel})}{c}$ versus c) yields linear behaviour over a wider range of the overlap parameter $c[\eta]$ than the Huggins plot (η_{red} versus c). This feature was noted to be particularly important for hydrophobic polymers, where significant deviations from linearity in the Huggins plot were observed for $[\eta]c \gtrsim 0.2$–0.3. Fitting the Huggins equation for larger values of the overlap parameter yielded artificially low values for the intrinsic viscosity and artificially high values for the Huggins coefficient. If the Kraemer equation was first used to estimate [η] and the Huggins equation was then applied with the value of the intrinsic viscosity determined by the Kraemer method, more accurate values of k_H were obtained. Note that these difficulties should disappear if measurements extend to sufficiently low $c[\eta]$, but this can be difficult to achieve experimentally, depending on the accuracy of the viscometer.

In the following, we examine the dependence of k_H and k_K on the charge fraction, degree of polymerisation, added salt concentration, and hydrophobicity for different polyelectrolyte systems. All the results discussed correspond to data obtained by dilute solutions with solvents of constant ionic strength. This differs from the isoionic dilution method, where the ionic strength of the solution (and not of the solvent) is kept constant. Such procedures yield much higher values of k_H, see for example refs. [41–44].

5.1 Influence of the charge fraction

Fig. 9 plots the dependence of the Huggins coefficient on the fraction of charged monomers for aminoacetalized polyvinyl alcohol (PVA) in 0.1 M K_2SO_4. The data are from Matsumoto and Eguchi.[36] The aminoacetalized PVA contains amine groups which are protonated by sulfuric acid. In ref. [36], the charge fraction was calculated assuming that one sulfuric acid molecule could protonate two amine groups. Given the weak dissociation constant of the second H^+ of sulfuric acid, here we assume each H_2SO_4 molecule protonates one amine group and calculate δ accordingly.

The Huggins constant is seen to decrease from a value of $\simeq 0.6$ at low charge fractions to $k_H \simeq 0.3$ at high charge fractions, as indicated by the dashed lines. The high-δ value falls below the $k_H \simeq 0.46$ value found for polymers in good solvent in a recent study.[45] In salt-free solutions, the opposite trend is observed: uncharged polymers display $k_H \simeq 0.3 - 0.8$ while polyelectrolytes display extremely high values of $k_H \simeq 10$, as discussed below.

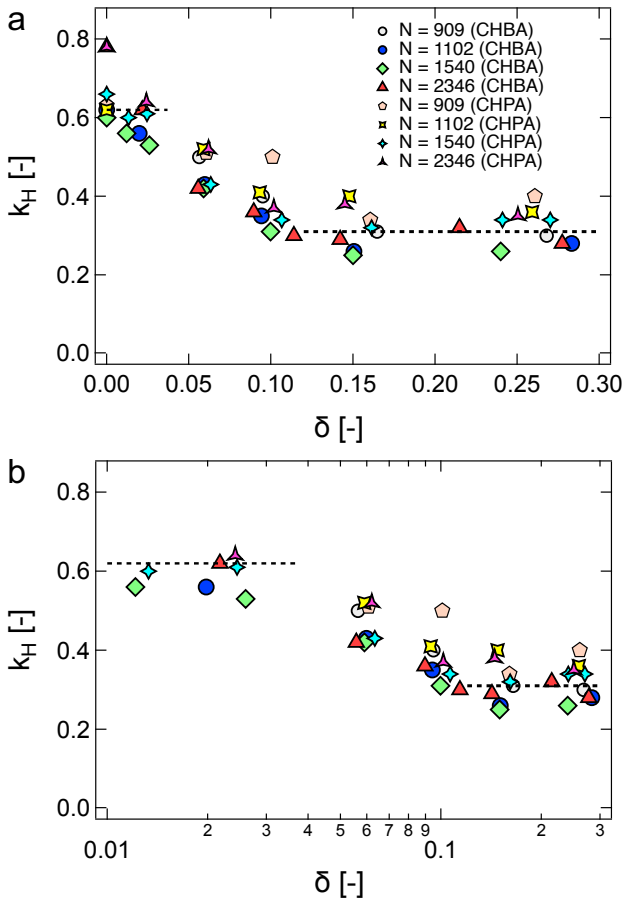

Fig. 9 Huggins coefficient of polyvinyl alcohol as a function of the fraction of charged monomers δ, see text for details. Degree of polymerisation and substitution method (see [36]) indicated in the legend. Data are extracted from ref. [36]. Top and bottom panels plot the same data.

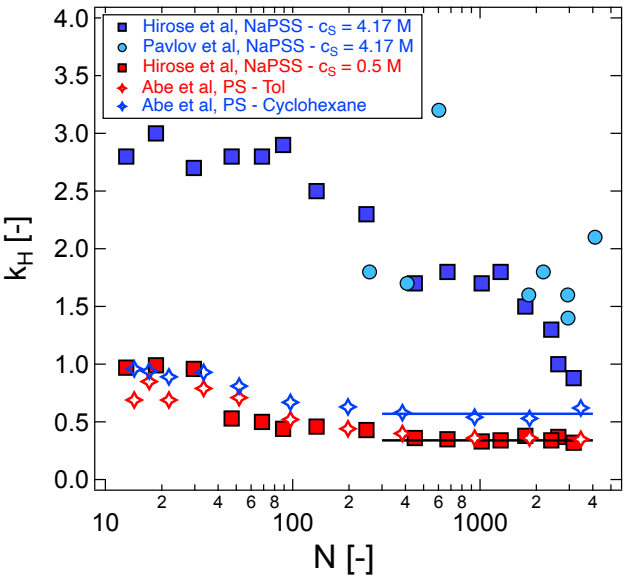

Fig. 10 Huggins coefficient as a function of degree of polymerisation for fully sulfonated NaPSS in excess added salt (full squares and circles), conditions are indicated on the legend. Data are from refs. [3,40] and references therein. Hollow stars are for polystyrene in toluene at $T = 15$ °C (good solvent) and cyclohexane at $T = 34.5$ °C (theta solvent) The dashed lines represent the values found for neutral polymers in good solvent ($k_H = 0.46$) and in θ solvent ($k_H = 0.96$), found in [45]. Solid line is high N value of $k_H = 0.34$.

5.2 Influence of molar mass

Fig. 10 plots the Huggins coefficient k_H of fully sulfonated NaPSS as a function of degree of polymerisation N. For $c_s = 0.5$ M the data (red squares) from Hirose et al.[3] display a decrease in k_H with increasing molar mass until reaching a plateau at $k_H \simeq 0.34$. The concentration range used to evaluate $[\eta]$ is not stated in ref. [3], however, given the excellent agreement in the values of $[\eta]$ (the intercept of the Huggins plot) between Hirose et a's data and results from other groups, as shown in the main text and in ref. [46], we conclude that measurements were carried out at sufficiently low values of $c[\eta]$. The data of Abe et al.[47] (red stars) for polystyrene in toluene at $T = 15$ °C (a good solvent) show a very similar trend. For $c_s = 4.17$ M, two data sets are considered: the results of Hirose et al., measured at $T = 17.5$ °C, corresponding to the theta point[3] and the results (blue circles) by Pavlov and co-workers,[40,48,49] measured at $T = 25$ °C, just above the theta point.

Pavlov and co-workers' data are more scattered, but broadly agree with Hirose et al's results. For comparison, the Huggins coefficient over the same range of N for polystyrene in cyclohexane at the theta point are included as blue stars. Here, PSS and PS, despite the identical solvent quality, as well as a similar persistence length, show very different values of k_H, particularly at low N values. The PSS data never reach a constant value, but appear to approach the neutral polymer limit toward the high N end of the dataset. The reason for the large differences in k_H between these two systems are not clear to us. The results highlight the difficulties in assigning a correlation between the solvent quality in a polymer-solvent system and the values of k_H. Such correlation, if it exists, probably holds only in the very high N limit. Note that for $N \lesssim 100$, where the conformation of the PS chain is identical in toluene and in cyclohexane, the k_H values do not converge. The values of the Huggins constant for PS good solvent ($k_H \simeq 0.34$) and in theta solvent ($k_H \simeq 0.57$) are lower than those found in a recent survey by Dobrynin et al.[45]

5.3 Influence of added salt

Fig. 11(a)–(b) plot the intrinsic viscosity $[\eta]$ and Huggins coefficient k_H of sodium polyacrylate in NaCl and NaBr solutions as a function of the added salt concentration c_s.

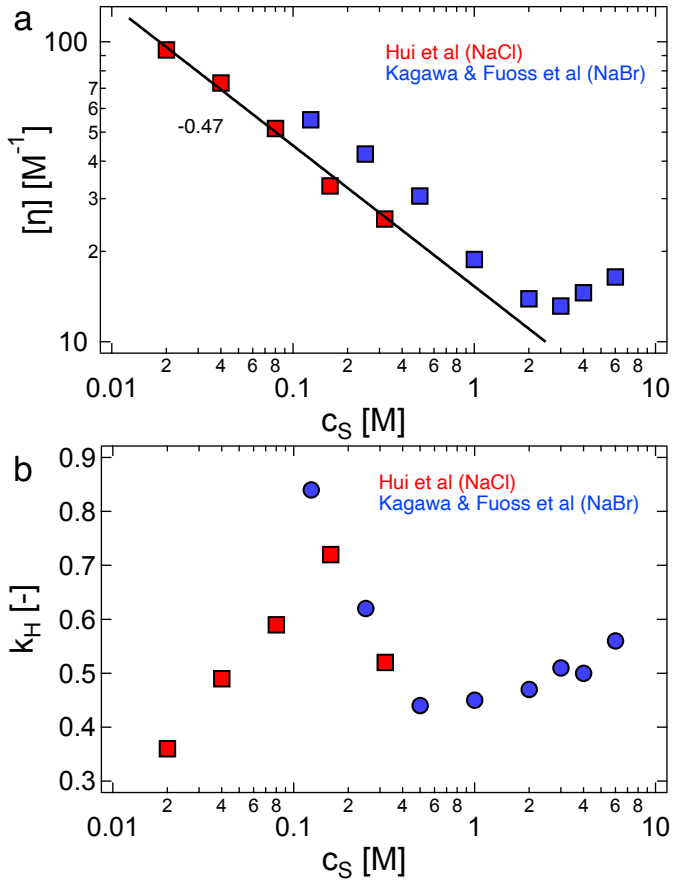

Fig. 11 Intrinsic viscosity (a) and Huggins coefficient (b) of sodium polyacrylate as a function of the added salt concentration c_s. Data are from refs. [50,51].

The data were reported in refs. [50,51]. The intrinsic viscosity follows a power law dependence with an exponent of -0.47, which is not far from the scaling prediction of -0.6, until $c_s \simeq 2$ M. At higher c_s, $[\eta]$ increases with increasing c_s, corresponding to an increase in the hydrodynamic volume of the chains, the origin of which remains unclear. For the relatively weak increases observed here, the trend beyond $c_S > 2$ M may be non-electrostatic in origin and instead be the result of improved solvent quality for the backbone. The Huggins coefficient for these samples, plotted in Fig. 11(b) shows a non-monotonic dependence on c_s. In the low c_s regime, k_H increases with increasing c_s. This is consistent with reports for other systems, as discussed below, and might stem from a reduction in the system's excluded volume. For neutral polymers, lower values of k_H are noticeable in good solvents compared to theta solvents. However, when higher concentrations of added salt are introduced, the trends of k_H reverse, initially decreasing, and then displaying a modest rise with c_s for values of c_s beyond 0.4 M. Notably, this non-monotonic relationship does not exhibit any evident correlation with the trends observed in the hydrodynamic size as discussed in Fig. 11(a).

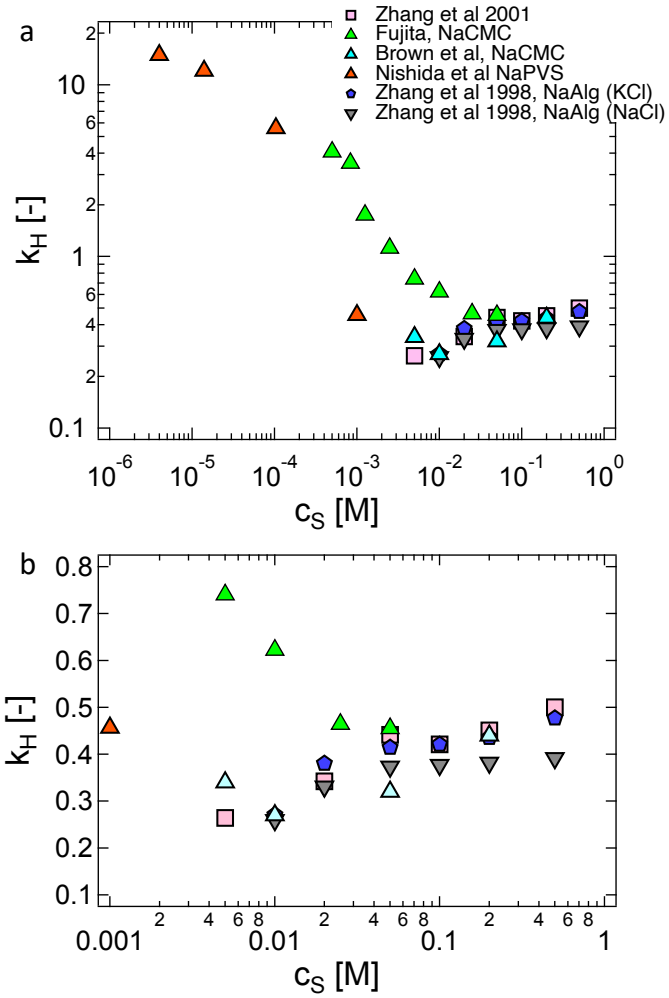

Fig. 12 Influence of added salt on the Huggins coefficient of various polyelectrolytes. The lower panel provides a closer view of the low k_H region. Data are from refs. [52–56].

Fig. 12 shows the influence of the added salt (type and concentration) on the Huggins coefficient of several polyelectrolyte systems, including data at very low c_s. A large upturn is observed at low c_s for the data of Nishida et al. for polyvinyl sulfate[55] and Fujita for carboxymethyl cellulose.[54] The data of Zhang et al.[52,53] for sodium alginate, which do not extend to such low added salt concentrations, show an increase in k_H with increasing c_s.

5.4 Influence of hydrophobicity

The influence of hydrophobic co-monomers on the Huggins coefficient of a sodium polyacrylate sample is considered in Fig. 13. Gosteva et al.[40] suggested that the Huggins plot may underestimate the value of $[\eta]$ and overestimate k_H if experiments were not carried out for sufficiently low values of the overlap parameter $[\eta]c$. This was found to be

particularly important for hydrophobic polymers. A procedure was proposed where the Kraemer method was first applied to obtain the intrinsic viscosity ($[\eta]_K$), and the Huggins equation was next fitted using $[\eta]=[\eta]_K$ while keeping k_H as the only free parameter. We re-analysed the data of Zhou et al.[51] for $c_s = 0.32$ M by using this procedure, see Tab. 1, and found that the Huggins constant differs by up to 60% obtained by using these two different procedures.

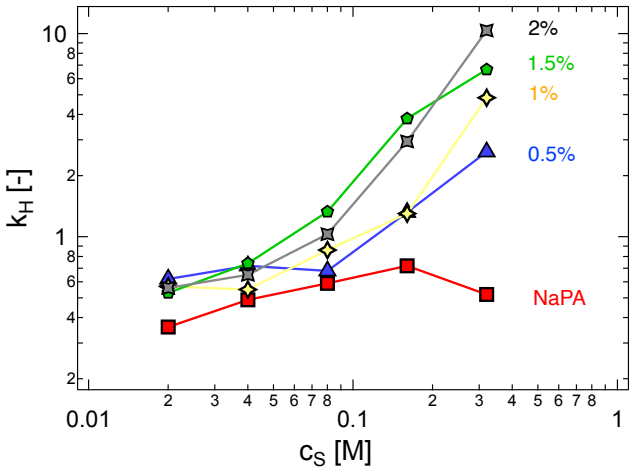

Fig. 13 dependence of Huggins coefficient on added salt for NaPA and for co-polymers of sodium acrylate and a hydrophobic co-monomer 2-(N-ethylperfluomctanesooctanesulfoamido) ethyl methacrylate (FMA). Numbers indicate the mol percent of FMA. Data are from ref. [51].

x_H	$[\eta]_H$ [dL/g]	$[\eta]_K$ [dL/g]	$[\eta]_H/[\eta]_K$ [-]	k_H [-]	k'_H [-]	k_K [-]
0	2.74	2.75	1.00	0.52	0.50	-0.038
0.5	2.82	3.09	0.91	2.89	2.08	1.07
1	1.94	2.15	0.90	5.12	3.60	2.33
1.5	1.21	1.29	0.94	7.19	5.74	4.46
2	1.38	1.63	0.85	11.75	7.34	5.40

Table 1 Viscosity parameters of dilute solution for polyacrylic acid in $c_s = 0.32$ M with varying mole fractions (x_H) of hydrophobic co-monomers. $[\eta]_H$ and $[\eta]_K$ are the intrinsic viscosity obtained by using the Huggins and Kraemer's method respectively. k_H is the Huggins coefficient obtained by fitting Eq. 1 with $[\eta]$ as a free parameter and k'_H when $[\eta]$ is fixed at the value obtained by the Kraemer plot. Values were obtained using data from ref. [51].

In the low c_s region, addition of the hydrophobic co-monomer 2-(N-ethylperfluomctanesooctanesulfoamido) ethyl methacrylate leads to a modest increase in k_H from 0.36 to 0.56. This is similar to the increases observed for neutral polymers when the solvent quality is lowered. At high added salt concentrations, k_H increases by more than an order of magnitude and takes values of $k_H \simeq 10$. In the high salt region, the intrinsic viscosity by contrast shows a weaker decrease by a factor of $\simeq \times 2$, corresponding to a decrease in the molecular dimensions by $\simeq 30\%$. This behaviour is likely related to the transition from expanded chains to compact micelle geometries as predicted by Dobrynin and Rubinstein for hydrophobically modified polyelectrolytes.[57] Similar trends were observed for polysoaps, see refs. [58,59].

5.5 Wolf equation

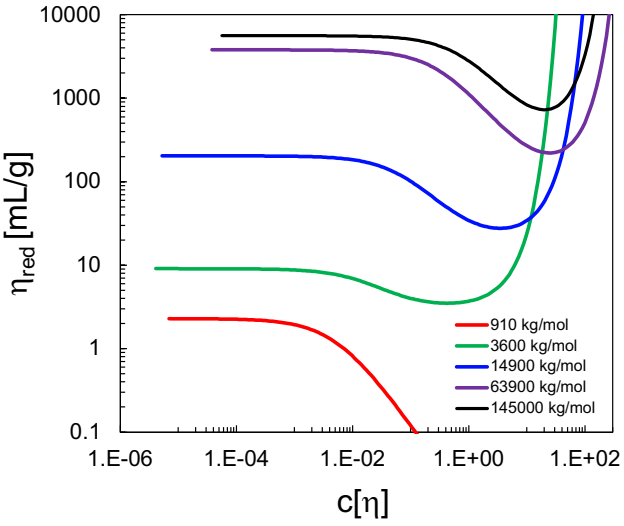

Fig. 14 Plots based on Eq. 3 using experimentally determined parameters[60] for different molar masses of NaPSS in DI water. Data are from ref. [60].

Wolf[61] used the following equation to fit the viscosity data of salt-free polyelectrolytes:

$$\ln(\eta/\eta_s) = \frac{c[\eta]+\lambda(c[\eta])^2}{1+\beta c[\eta]+\gamma(c[\eta])^2}, \qquad (3)$$

where η_s is the solvent viscosity, $[\eta]$ is the intrinsic viscosity, β, γ and λ are fit parameters which depend on the molar mass of the polymer and the added salt concentration. The quadratic term in the denominator is generally not needed to fit experimental data if only dilute concentrations are considered. The reduced viscosity of NaPSS calculated from Eq. 3 and the fit parameters obtained in ref. [60] for NaPSS with different molecular weights are plotted as a function of the overlap parameter in Fig. 14. The plots do not show a peak in η_{red} vs. c curves. We therefore conclude that Eq. 3 does not describe the concentration dependence of η_{red} over the entire concentration regime and is likely to overestimate the values of $[\eta]$, as is the case with Fuoss' method, described in the main text.

6 Molar mass and c_s scaling of k_D

Dynamic light scattering from polymer solutions can be used to measure an apparent diffusion coefficient $D(c)$ for dilute polymer solutions. Extrapolation to $c \to 0$ yields the translational diffusion coefficient D. In the dilute limit, the apparent diffusion coefficient varies linearly with the polymer concentration.

$$D(c) \simeq D(1 + k_D c), \tag{4}$$

where D is the single-chain translational diffusion coefficient of the chains in the infinite dilution limit and k_D is known as the diffusion virial coefficient or the diffusion interaction parameter.[62]

A related constant is k_s, which describes the concentration dependence of the friction factor (f_r) of the macromolecules:

$$f_r = f_{r,0}(1 + k_s c),$$

where $f_{r,0}$ is the friction factor at infinite dilution.

The constant k_D is related to k_s and the second virial coefficient as:[76]

$$k_D + k_S = 2A_2M - \overline{v},$$

where $\overline{v}$ is the partial specific molar volume. Several authors have evaluated the above relationship, have found it to hold within the margins of experimental error.[77]

In the high M limit, $k_D \simeq 2A_2M - k_S$. The theories of Pyun and Fixman[78] and Yamakawa[79] expect $k_s \propto A_0[\eta]$, where $A_0 \simeq 1.4 - 1.6$, depending on several assumptions, see ref. [76] for details. Noting that in the high M limit $A_2M \simeq 1.2[\eta]$ (see Fig. 29(a) in the main manuscript), the ratio $k_D/(A_2M)$ is expected to take a value close to unity in the good solvent limit. Near the theta point, Yamakawa's theory expects $k_D \simeq -0.2[\eta]$ for Gaussian chains in the high-M limit.[76]

The dependencies of k_D on degree of polymerisation and added salt concentration for various polyelectrolyte systems are plotted on Figs. 15(a)–(b) using data from refs. [63–75]. Broadly, a dependence of $k_D \sim N^{0.78}/c_s$ was observed, although departures from this scaling for several systems were clear. The ratio of k_D to the product of the second virial coefficient and the molar mass of several polyelectrolytes is shown to be approximately independent of degree of polymersiation in Fig. 15(c) for NaPSS, NAPA. Data for NAPSMS on the other hand showed an increase of this ratio with N. The added salt concentration dependence of $k_D/(A_2M_w)$ is considered in Fig. 15(d), which shows a modest dependence of $k_D/(A_2M_w)$ on c_s. The results in Fig. 15(c)–(d) suggest that k_D is approximately proportional to the overlap concentration of polyelectrolyte chains in the presence of excess added salt. The theories

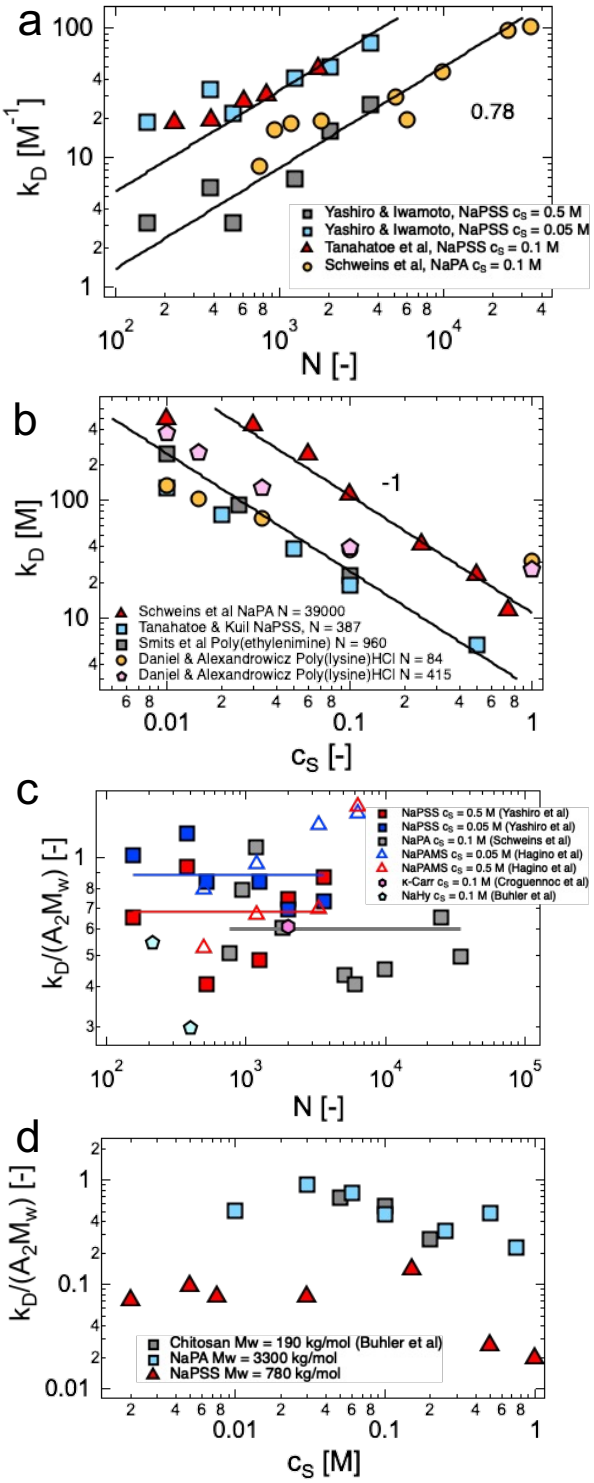

Fig. 15 Diffusion second virial coefficient as a function of (a) polymer degree of polymerisation and (b) added salt. Lines are power-laws with the exponent indicated on the panel. Ratio $k_D/(A_2M_w)$ as a function of (c) polymer degree of polymerisation and (c) added salt concentration. Lines in plot (d) are average values for Yashiro et al.'s NaPSS data and Schweins et al.'s NaPA data. Data are from refs. [63–75].

proposed by Pyun and Fixman, as well as Yamakawa, anticipate this proportional relationship, which is consistent with experimental observations for neutral polymers in a good solvent. However, in certain systems, the observed values of $k_D/(A_2M_w) \simeq 0.1$ are considerably lower than anticipated. It remains unclear whether this discrepancy is attributable to shortcomings in the theoretical frameworks or potential errors in the experimental data.

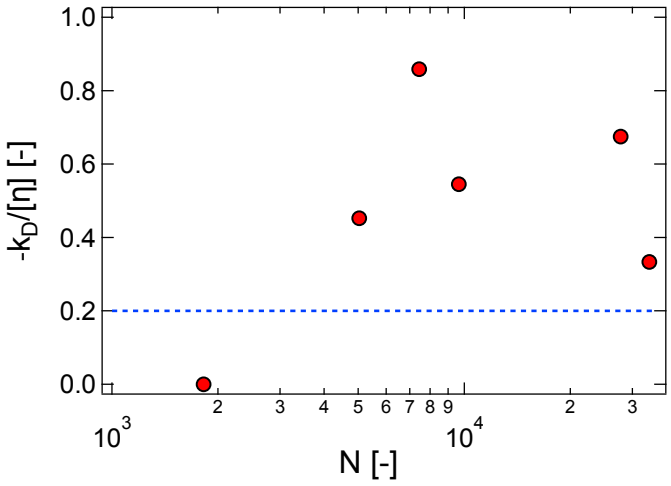

Fig. 16 Ratio between $-k_D$ and the intrinsic viscosity of NaPA at the theta point (1.5 M NaBr). The intrinsic viscosity is estimated from R_H data and Eq. 55 in the main manuscript with $U_{\eta f} = 0.12$. Data are from ref. [63].

Yamakawa's prediction of $k_D \simeq -0.2[\eta]$ ideal chains is tested in Fig. 16. As there are no published data for the intrinsic viscosity and diffusion virial coefficient for any polyelectrolyte, we use Schweins and Huber's[63] results for NaPA in 1.5 M NaBr and estimate the intrinsic viscosity of their polymers from Eq. 55 of the main text using the reported values of R_H. The ratio $-k_D/[\eta]$ is plotted as a function of molar mass, and no obvious trend is observed. The average value for the highest five molar masses is $\simeq 0.5$. Running the same analysis for poly(methyl methacylate) (PMMA), poly(isobutylene) (PIB) and polystyrene (PS) in theta solvent gives values of $0.7-0.9$ for PMMA, 0.5 for PS and 0.8 for PIB.

7 Properties of polystyrene in dilute solutions

Figs. 17 plots the radius of gyration of polystyrene in good solvent (Toluene at $T = 288-298$ K) and in theta solvent (Cyclohexane at $T = 307.65$ K). The data are extracted from various references, compiled by Fetters et al.,[80] where M_w and R_g are measued by static light scattering. For low molar masses, which were not included in Fetters et al.'s compilation, we use the data of Huber et al.[81], Konishi et al.[82]

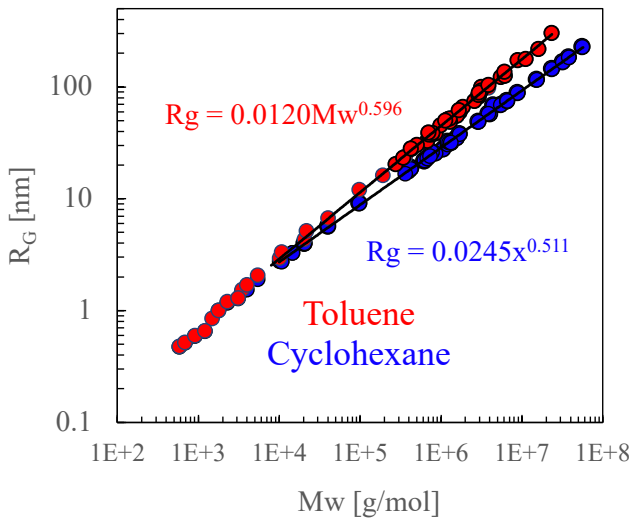

Fig. 17 Radius of gyration of polystyrene in toluene and cyclohexane. Data are from ref. [80] and references therein and refs. [47,81–83]. Lines are best-fit power-laws.

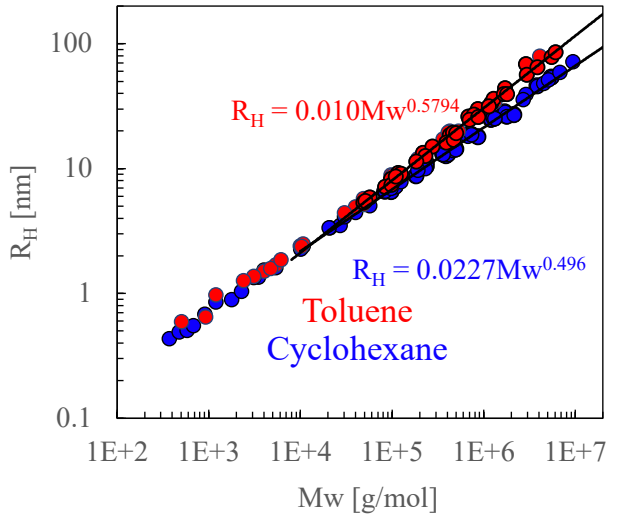

Fig. 18 Hydrodynamic radius of polystyrene in toluene and cyclohexane. Data are from ref. [80] and references therein and refs. [47,81,83–86]. Lines are best-fit power-laws.

and Abe et al.[47] Measuring the radius of gyration of short polymer chains with SLS is challenging due to the weak angular dependence of the scattered radiation over the accessible q range. Huber et al. determined the weight-averaged molar mass with static light scattering and the radius of gyration by using small angle neutron scattering (SANS). Abe et al. used small angle x-ray scattering (SAXS) to determine the radius of gyration of short polystyrene chains in Toluene (T = 288K) or cyclohexane at the theta point. Note that Abe et al. reported two values for the radius of gyration: 1) the true radius of gyration (R_g), obtained from the slope of the Berry plot and 2) the radius of gyration cor-

rected to suppress the influence of the finite lateral dimensions of the chain. We plot the former value in Fig. 17. Details of the experimental methods for determining the molar mass and radius of gyration of short polystyrene chains using SAXS are discussed in detail in ref. [82].

A similar plot for the hydrodynamic radius as a function of molar mass is shown in Fig. 18. Data follow the compilation of Fetters et al.[80] and also references [47,81,83–86]. Power-law exponents for ideal and expanded chains are also observed.

The second virial coefficient of polystyrene in toluene is plotted in Fig. 19 as a function of molar mass. As before, we use the values collected by Fetters et al. from various studies and combine them with the data from Yamakawa and co-workers and Huber et al.[47,81,87] A best-fit power-law for $M_w > 10000$, corresponding to chains larger than the thermal blob size yields an exponent of -0.258, slightly larger than the scaling prediction in the high excluded volume limit ($A_2 \sim R^3/M \sim M^{-0.23}$). For cyclohexane, the second virial coefficient is essentially zero at high molar masses and takes a positive value for short chains, see [88](these results are not plotted here). The deviation to higher values observed at lower molar masses was assigned by Yamakawa and co-workers to the influence of chain ends.

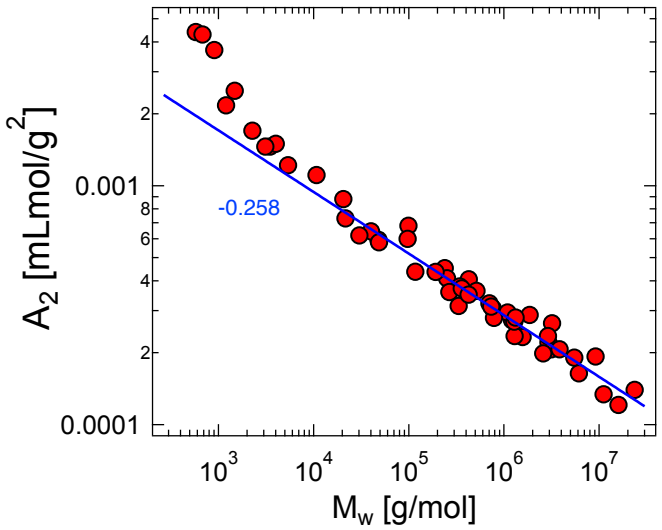

Fig. 19 Second virial coefficient of polystyrene in toluene. Data are from ref. [80] and references therein and refs. [47,81,87]. Line is best-fit power-law excluding low M_w data.

The intrinsic viscosity of polystyrene in toluene and cyclohexane as a function of molar mass are compared in Fig. 20. Most of the data are collected by Fetters et al. [80] and we also include results from refs. [47,89] which extend the molar mass range. The datasets from the different studies agree well.

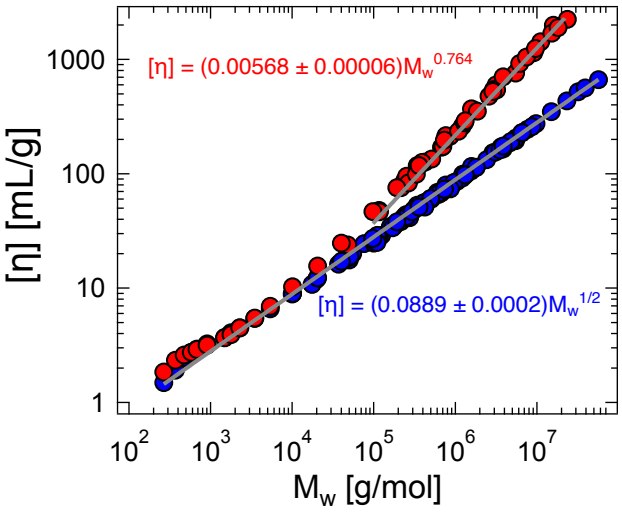

Fig. 20 Intrinsic viscosity of polystyrene in toluene (red symbols) and cyclohexane (blue symbols). Data are from ref. [80] and references therein and refs. [47,89]. Lines are power-law fits with exponent fixed to theoretical values for good and θ solvent values.

8 Universal ratios for polystyrene solutions

8.1 The ρ ratio

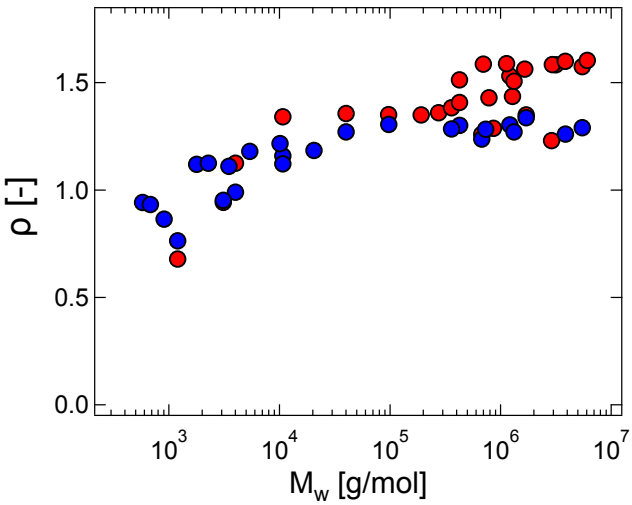

Fig. 21 Ratio of radius of gyration to hydrodynamic radius of polystyrene in toluene (red symbols) and cyclohexane (blue symbols). Data are from [47,80,81,89].

The ratio of the radius of gyration and hydrodynamic radius $\rho = R_g/R_H$ for polystyrene in toluene and cyclohexane is plotted as a function of the molar mass in Fig. 21, using the same data as in Fig. 17 and 18 for which values of R_g and R_H are available for the same sample. Given the limited number of points available, it is not possible to reliably estimate the high M plateau. Therefore, in Figs. 22

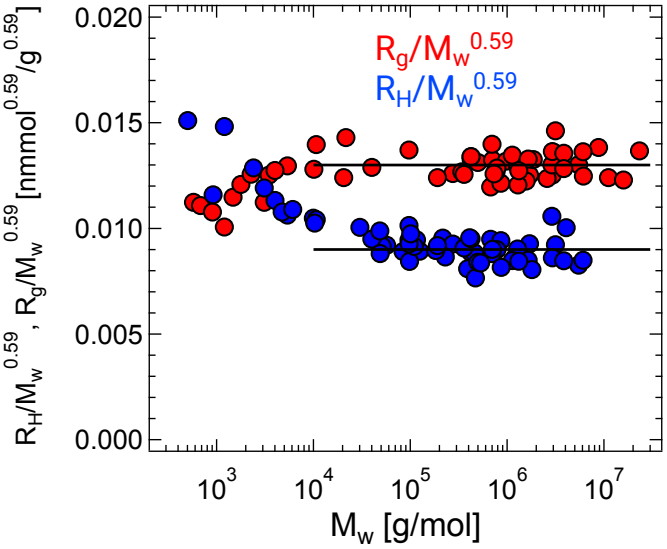

Fig. 22 Radius of gyration and hydrodynamic radius of polystyrene in toluene, normalised by $M_w^{0.59}$. Data are from refs. in figs. 18 and 17.

and 23, we compute the values of R_g and R_H normalised by their M_w scaling in the long polymer limit ($M_w^{1/2}$ in theta solvent and $M_w^{0.59}$ in good solvent). The parameter ρ can be estimated from the average values of the high-M_w limit ($M_w > 25$ kg/mol for cyclohexane and $M_w > 40$ kg/mol for toluene), indicated by the black lines in figures 22 and 23. The resulting values are listed in table 4 of the main manuscript.

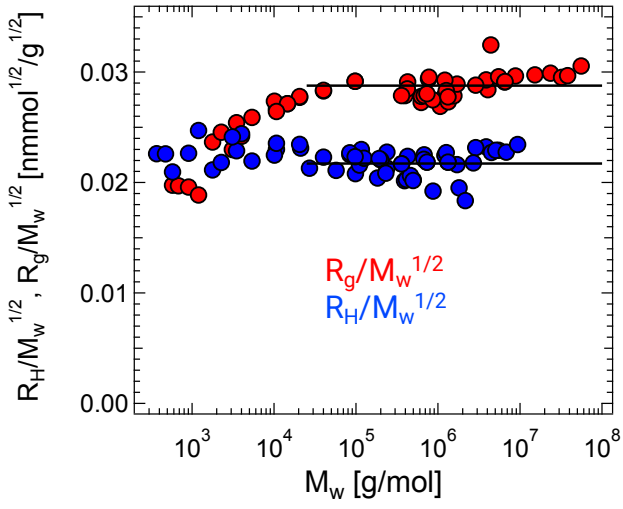

Fig. 23 Radius of gyration and hydrodynamic radius of polystyrene in cyclohexane normalised by $M_w^{1/2}$. Data are from refs. in figs. 18 and 17.

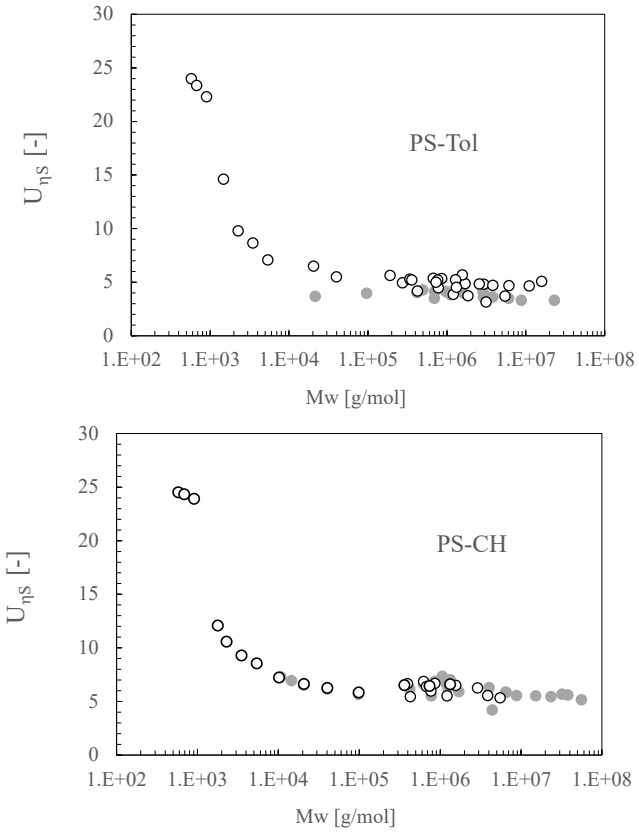

Fig. 24 Flory viscosity factor for polystyrene in good solvent (top) and theta solvent (bottom). Open circles are calculated from the measured R_g and $[\eta]$ data-points. Closed symbols use interpolated values of $[\eta]$, based on Fig. 20. Data are from ref. [80] and references therein and refs. [47,89]. The high M values are $U_{\eta S} = 4.8 \pm 0.1$ in toluene and $U_{\eta S} = 6.1 \pm 0.1$ in cyclohexane. The confidence intervals are standard errors.

8.2 The Flory-Fox viscosity ratio

The Fox-Flory viscosity ratio of polystyrene in toluene and in cyclohexane is plotted as a function of molar mass in Fig. 24. Hollow white symbols are data for which R_g and $[\eta]$ are measured directly. Closed grey symbols use an interpolated value of $[\eta]$, based on the power-law fit to the data in Fig. 20. Both methods yield consistent results.

The high molar mass value of Φ for polystyrene in toluene is found to be $U_{\eta S} = 4.8 \pm 0.1$ for datasets where R_g and $[\eta]$ values directly (hollow circles in figure 24). For values where only R_g data are available and $[\eta]$ is interpolated from a power-law fit (grey circles in figure 24), a lower value of 3.89 ± 0.08. For cyclohexane, both datasets agree: 6.1 ± 0.1 for the hollow circles and 6.1 ± 0.2 for the gray circles.

9 Influence of added salt on the ρ-ratio

Fig. 25 depicts the influence of added salt concentration on the ρ ratio of NaPSS. The results of Norisuye and co-

workers[3,65,69] represent averages across all measured molar masses, while the remaining data pertains to individual molar masses. The datasets of Raziel and Eisenberg, and Nordmeier show a monotonic decrease of ρ with c_S. These results are in line with the two points from Norisuye and co-workers's data and the trends observed for other systems[63,90] (see below). The exception are Borochov and Eisenberg's data, which show a non-monotonic dependence with c_S. This unusual behaviour may simply be the result of experimental error.

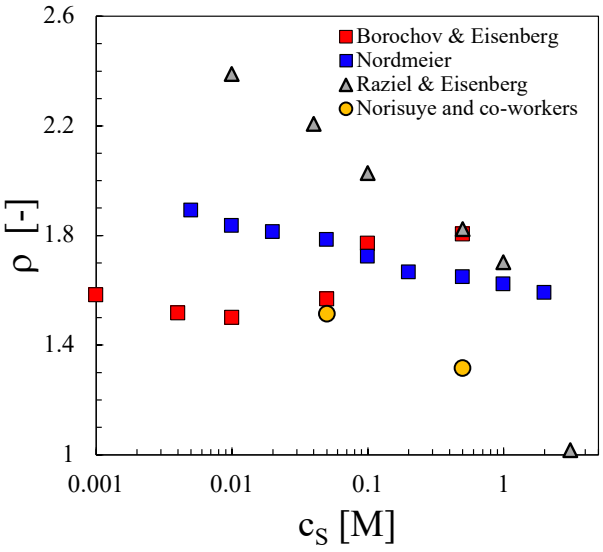

Fig. 25 Ratio of radius of gyration to hydrodynamic radius of polystyrene sulfonate in aqueous salt solutions. Data are from refs. [3,4,65,69,91,92].

The ratio ρ for the NaPA sample considered in figure 21 of the main text is plotted as a function of the added salt concentration in Fig. 26. The value decreases from $\simeq 2.1$ for the lowest c_s reported, to $\simeq 1.45$ at the theta salt point. These values exceed those observed for PS in good and theta solvents, likely, in part due to the modest polydispersity of the NaPA sample. The measured value of R_g through light scattering represents a z-average, and it is more significantly influenced compared to R_H measured by DLS, which corresponds to an inverse z-average. Data by Beer et al for quaternised vinylpyridinium) are included for comparison and show a similar trend.

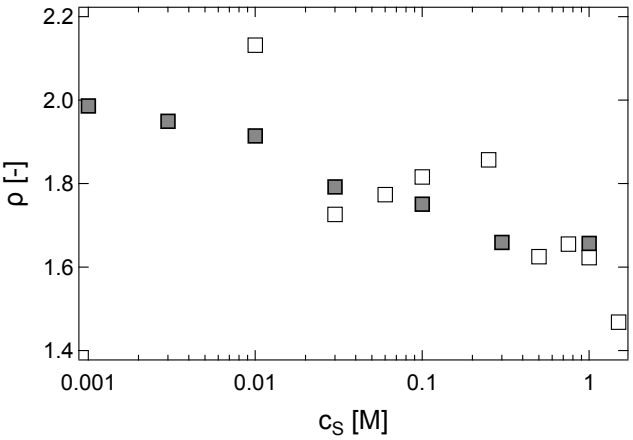

Fig. 26 Ratio of radius of gyration to hydrodynamic radius as a function of added salt. Hollow squares are for the same sodium polyacrylate sample considered on Figure 21 of the main text. Data are from [63]. Full symbols are for quaternised poly(vinylpyridinium), data are from [90].

References

1 M. Rubinstein and R. H. Colby, *Polymer Physics*, Oxford University Press: New York, 2003.

2 H. Eisenberg and D. Woodside, *The Journal of Chemical Physics*, 1962, **36**, 1844–1854.

3 E. Hirose, Y. Iwamoto and T. Norisuye, *Macromolecules*, 1999, **32**, 8629–8634.

4 E. Nordmeier and W. Dauwe, *Polym. J.*, 1992, **24**, 229–238.

5 A. Takahashi and M. Nagasawa, *J. Am. Chem. Soc.*, 1964, **86**, 543–548.

6 A. Raziel, *Excluded volume study of polyelectrolyte solutions: Potassium polystyrenesulfonate*, The Weizmann Institute of Science (Israel), 1971.

7 R. Buscall and T. Corner, *Eur. Polym. J.*, 1982, **18**, 967–974.

8 P. J. Flory and J. E. Osterheld, *J. Phys. Chem.*, 1954, **58**, 653–661.

9 N. Borochov and H. Eisenberg, *Biopolymers: Original Research on Biomolecules*, 1984, **23**, 1757–1769.

10 I. Sabbagh and M. Delsanti, *The European Physical Journal E*, 2000, **1**, 75–86.

11 R. Schweins, G. Goerigk and K. Huber, *Eur. Phys. J. E*, 2006, **21**, 99–110.

12 N. Volk, D. Vollmer, M. Schmidt, W. Oppermann and K. Huber, *Polyelectrolytes with Defined Molecular Architecture II*, 2004, 29–65.

13 M. A. Axelos, M. M. Mestdagh and J. Francois, *Macromolecules*, 1994, **27**, 6594–6602.

14 V. Prabhu, M. Muthukumar, G. Wignall and Y. Melnichenko, *Polymer*, 2001, **42**, 8935–8946.

15 V. Prabhu, M. Muthukumar, G. D. Wignall and Y. B. Melnichenko, *J. Chem. Phys.*, 2003, **119**, 4085–4098.

16 V. M. Prabhu, *Phase behavior of polyelectrolyte solutions*, University of Massachusetts Amherst, 2002.

17 W. N. Sharratt, R. OÃ¢ÂÂConnell, S. E. Rogers, C. G. Lopez and J. T. Cabral, *Macromolecules*, 2020, **53**,

1451–1463.
18 S. Kanai and M. Muthukumar, *The Journal of chemical physics*, 2007, **127**, year.
19 T. YANAKI and M. YAMAGUCHI, *Chemical and pharmaceutical bulletin*, 1994, **42**, 1651–1654.
20 M. Fixman, *The Journal of Chemical Physics*, 1966, **45**, 793–803.
21 K. Tsutsumi and T. Norisuye, *Polym. J.*, 1998, **30**, 345–349.
22 J. Cohen, Z. Priel and Y. Rabin, *J. Chem. Phys.*, 1988, **88**, 7111–7116.
23 J. Cohen and Z. Priel, *J. Chem. Phys.*, 1990, **93**, 9062–9068.
24 J. Yang, N. Liu, D. Yu, C. Peng, H. Liu, Y. Hu and J. Jiang, *Industrial & engineering chemistry research*, 2005, **44**, 8120–8126.
25 W. Essafi, N. Haboubi, C. Williams and F. Boué, *J. Phys. Chem. B*, 2011, **115**, 8951–8960.
26 H. Vink, *Die Makromolekulare Chemie: Macromolecular Chemistry and Physics*, 1970, **131**, 133–145.
27 H. Vink, *Polymer*, 1992, **33**, 3711–3716.
28 J. Yamanaka, S. Yamada, N. Ise and T. Yamaguchi, *J. Polym. Sci. B: Polym. Phys.*, 1995, **33**, 1523–1526.
29 D. C. Boris and R. H. Colby, *Macromolecules*, 1998, **31**, 5746–5755.
30 J. L. Ganter, M. Milas and M. Rinaudo, *Polymer*, 1992, **33**, 113–116.
31 S. Batzill, R. Luxemburger, R. Deike and R. Weber, *The European Physical Journal B-Condensed Matter and Complex Systems*, 1998, **1**, 491–501.
32 J. A. V. Butler, A. Robins and K. Shooter, *Proceedings of the Royal Society of London. Series A. Mathematical and Physical Sciences*, 1957, **241**, 299–310.
33 I. Roure, M. Rinaudo, M. Milas and E. Frollini, *Polymer*, 1998, **39**, 5441–5445.
34 A. Gulati, M. Jacobs, C. G. Lopez and A. V. Dobrynin, *Macromolecules*, 2023, **56**, 2183–2193.
35 R. Borsali, T. Vilgis and M. Benmouna, *Macromolecules*, 1992, **25**, 5313–5317.
36 M. Matsumoto and T. Eguchi, *Journal of Polymer Science*, 1957, **23**, 617–634.
37 M. L. Huggins, *Journal of the American Chemical Society*, 1942, **64**, 2716–2718.
38 J. Yamanaka, H. Araie, H. Matsuoka, H. Kitano, N. Ise, T. Yamaguchi, S. Saeki and M. Tsubokawa, *Macromolecules*, 1991, **24**, 6156–6159.
39 E. O. Kraemer, *Industrial & Engineering Chemistry*, 1938, **30**, 1200–1203.
40 A. Gosteva, A. S. Gubarev, O. Dommes, O. Okatova and G. M. Pavlov, *Polymers*, 2023, **15**, 961.
41 H. Inagaki, H. Sakurai and T. Sasaki, *Bulletin of the Institute for Chemical Research, Kyoto University*, 1956, **34**, 74–86.
42 R. Davis and W. Russel, *Macromolecules*, 1987, **20**, 518–525.
43 Y. Mylonas, G. Staikos and M. Ullner, *Polymer*, 1999, **40**, 6841–6847.
44 G. Staikos and G. Bokias, *Polym. Int.*, 1993, **31**, 385–389.
45 A. V. Dobrynin, R. Sayko and R. H. Colby, *ACS Macro Letters*, 2023, **12**, 773–779.
46 C. G. Lopez, J. Linders, C. Mayer and W. Richtering, *Macromolecules*, 2021, **54**, 8088–8103.
47 F. Abe, Y. Einaga, T. Yoshizaki and H. Yamakawa, *Macromolecules*, 1993, **26**, 1884–1890.
48 G. M. Pavlov, A. A. Gosteva, O. V. Okatova, O. A. Dommes, I. I. Gavrilova and E. F. Panarin, *Polymer Chemistry*, 2021, **12**, 2325–2334.
49 G. Pavlov and A. Gosteva, *Polymer Science, Series A*, 2022, **64**, 586–590.
50 I. Kagawa and R. M. Fuoss, *J. Polym. Sci.*, 1955, **18**, 535–542.
51 Z. Hui, S. Guo-Qiang, Z. Yun-Xiang, R. Ma, Deeing and L. H. Lukas, *Chinese Journal of Chemistry*, 2000, **18**, 322–327.
52 H. Zhang, H. Zheng, Q. Zhang, J. Wang and M. Konno, *Biopolymers: Original Research on Biomolecules*, 1998, **46**, 395–402.
53 H. Zhang, H. Wang, J. Wang, R. Guo and Q. Zhang, *Polymers for Advanced Technologies*, 2001, **12**, 740–745.
54 H. Fujita and T. Homma, *J. Polym. Sci.*, 1955, **15**, 277–295.
55 K. Nishida, K. Kaji, T. Kanaya and N. Fanjat, *Polymer*, 2002, **43**, 1295–1300.
56 W. Brown, D. Henley and J. Ohman, *Arkiv Kemi*, 1964, **22**, 189–206.
57 A. V. Dobrynin and M. Rubinstein, *Macromolecules*, 2000, **33**, 8097–8105.
58 U. P. Strauss, N. L. Gershfeld and E. H. Crook, *The Journal of Physical Chemistry*, 1956, **60**, 577–584.
59 H. Inoue, *Kolloid-Zeitschrift und Zeitschrift für Polymere*, 1964, **195**, 102–110.
60 J. Eckelt, A. Knopf and B. A. Wolf, *Macromolecules*, 2008, **41**, 912–918.
61 B. A. Wolf, *Macromol. Rapid Commun.*, 2007, **28**, 164–170.
62 J. F. Douglas, R. Curtis, P. S. Sarangapani, S. D. Hudson, R. L. Jones and J. A. Pathak, *Biophysical Journal*,

2017, **113**, 753–754.
63 R. Schweins, J. Hollmann and K. Huber, *Polymer*, 2003, **44**, 7131–7141.
64 E. Daniel and Z. Alexandrowicz, *Biopolymers: Original Research on Biomolecules*, 1963, **1**, 473–495.
65 J. Yashiro and T. Norisuye, *J. Polym. Sci. B: Polym. Phys.*, 2002, **40**, 2728–2735.
66 R. Hagino, J. Yashiro, M. Sakata and T. Norisuye, *Polym. J.*, 2006, **38**, 861–867.
67 J. Yashiro and T. Norisuye, *Polym. Bull.*, 2006, **56**, 467–474.
68 J. Yashiro, R. Hagino, S. Sato and T. Norisuye, *Polym. J.*, 2006, **38**, 57–63.
69 Y. Iwamoto, E. Hirose and T. Norisuye, *Polymer J.*, 2000, **32**, 428–434.
70 J. Tanahatoe and M. Kuil, *J. Phys. Chem. A*, 1997, **101**, 8389–8394.
71 J. Tanahatoe and M. Kuil, *Macromolecules*, 1997, **30**, 6102–6106.
72 R. Smits, M. Kuil and M. Mandel, *Macromolecules*, 1993, **26**, 6808–6816.
73 E. Buhler and M. Rinaudo, *Macromolecules*, 2000, **33**, 2098–2106.
74 R. M. Peitzsch, M. J. Burt and W. F. Reed, *Macromolecules*, 1992, **25**, 806–815.
75 E. Buhler, O. Guetta and M. Rinaudo, *Int. J. Polym. Anal. Charact.*, 2001, **6**, 155–175.
76 H. Yamakawa, *Modern theory of polymer solutions*, Harper & Row, 1971.
77 T. Nicolai and M. Mandel, *Macromolecules*, 1989, **22**, 2348–2356.
78 C. Pyun and M. Fixman, *The Journal of Chemical Physics*, 1964, **41**, 937–944.
79 H. Yamakawa, *The Journal of Chemical Physics*, 1962, **36**, 2995–3001.
80 L. Fetters, N. Hadjichristidis, J. Lindner and J. Mays, *J. Phys. Chem. Ref. Data*, 1994, **23**, 619–640.
81 K. Huber, S. Bantle, P. Lutz and W. Burchard, *Macromolecules*, 1985, **18**, 1461–1467.
82 T. Konishi, T. Yoshizaki, T. Saito, Y. Einaga and H. Yamakawa, *Macromolecules*, 1990, **23**, 290–297.
83 T. Yamada, T. Yoshizaki and H. Yamakawa, *Macromolecules*, 1992, **25**, 377–383.
84 J. Szydlowski and W. A. Van Hook, *Macromolecules*, 1998, **31**, 3266–3274.
85 J. Rauch and W. Köhler, *J. Chem. Phys.*, 2003, **119**, 11977–11988.
86 T. Arai, F. Abe, T. Yoshizaki, Y. Einaga and H. Yamakawa, *Macromolecules*, 1995, **28**, 3609–3616.
87 Y. Einaga, F. Abe and H. Yamakawa, *Macromolecules*, 1993, **26**, 6243–6250.
88 H. Yamakawa, F. Abe and Y. Einaga, *Macromolecules*, 1994, **27**, 5704–5712.
89 F. Abe, Y. Einaga and H. Yamakawa, *Macromolecules*, 1993, **26**, 1891–1897.
90 M. Beer, M. Schmidt and M. Muthukumar, *Macromolecules*, 1997, **30**, 8375–8385.
91 A. Raziel and H. Eisenberg, *Isr. J. Chem.*, 1973, **11**, 183–199.
92 N. Borochov and H. Eisenberg, *Macromolecules*, 1994, **27**, 1440–1445.